Rock Mechanics and Rock Engineering (2021) 54:1431–1447
https://doi.org/10.1007/s00603-020-02318-6

ORIGINAL PAPER

Pull-out and Critical Embedment Length of Grouted Rebar Rock Bolts-Mechanisms When Approaching and Reaching the Ultimate Load

Are Håvard Høien[1] · Charlie C. Li[2] · Ning Zhang[3]

Received: 25 March 2020 / Accepted: 17 November 2020 / Published online: 2 January 2021

Abstract

Rock bolts are one of the main measures used to reinforce unstable blocks in a rock mass. The embedment length of fully grouted bolts in the stable and competent rock stratum behind the unstable rock blocks is an important parameter in determining overall bolt length. It is required that the bolt section in the stable stratum must be longer than the critical embedment length to ensure the bolt will not slip when loaded. Several series of pull tests were carried out on fully grouted rebar bolts to evaluate the pull-out mechanics of the bolts. Bolt specimens with different embedment lengths and water/cement ratios were installed in either a concrete block of one cubic meter or in steel cylinders. Load displacement was recorded during testing. For some of the bolts loaded beyond the yield load, permanent plastic steel deformation was also recorded. Based on the test results, three types of failure mechanisms were identified, corresponding to three loading conditions: (1) pull-out below the yield strength of the bolt steel; (2) pull-out between the yield and ultimate loads, that is, during strain hardening of the steel; and (3) steel failure at the ultimate load. For failure mechanisms 2 and 3, it was found that the critical embedment length of the bolt included three components: an elastic deformation length, a plastic deformation length and a completely debonded length due to the formation of a failure cone at the borehole collar.

Keywords Bolt pull-out · Rock bolts · Embedment length · Rock support

List of symbols

A_{gt}	Strain at the ultimate force
d_b	Bolt diameter
F	Load
F_u	Steel ultimate load/strength
F_y	Steel yield load/strength
$F(s)$	Force at a given strain
$F(s_s)$	Force at the start of a segment
$F(s_e)$	Force at the end of a segment
l_0	Segment length before testing
l_1	Segment length after testing
L	Embedment length
L_{CE}	Critical elastic embedment length
L_{CP}	Critical plastic embedment length
L_E	Plastic embedment length
L_{NB}	No bound length (cone length)
L_P	Plastic embedment length
L_S	Segment length
L_{TC}	Total critical embedment length
s	Strain
S	Bolt displacement
$\sigma(s)$	Stress at a given strain
$\sigma(x)$	Stress at position x in the plastic embedded zone
σ_y	Yield stress
σ_u	Ultimate yield stress
τss	Average shear strength
τ_m	Maximum bond shear strength
τ_{Rmax}	Maximum residual shear strength
τ_{Rmin}	Minimum residual shear strength
τ_{ss}	Average residual shear strength

✉ Are Håvard Høien
are.hoien@vegvesen.no

[1] Norwegian Public Roads Administration, Oslo, Norway

[2] Norwegian University of Science and Technology (NTNU), Trondheim, Norway

[3] North China Electric Power University, Beijing, China

1 Introduction

Rock bolts are the most crude and basic rock support measure for stabilising rock surfaces. There are numerous different designs and dimensions of rock bolts, from simple grouted rebar bolts to highly specialised bolts used to manage different types of rock mass conditions and behaviours. The fully grouted rebar rock bolt however, is the most commonly used in practice.

A rebar bolt can be integrated into a rock mass using a grout bond along its entire length. The bond strength is often represented by the so-called pull-out strength, which is the average shear strength in the rock-grout or bolt-grout interface. The embedment length of bolt samples used for such tests is usually short, less than 20 cm, and the bolt bar is therefore loaded below its yield strength (F_y) with elastic deformations (Kılıc et al. 2002). If the encapsulated segment of a rock bolt exceeds the critical embedment length, plastic deformation occurs in the bolt bar before rupture (Li et al. 2016b).

The critical embedment length is an important parameter, for instance, when deciding the length of grouted rock bolts behind potentially unstable rock joints or the anchoring length of the bolts. Most rock bolts on site have extensive embedment lengths and in extreme cases, when loaded above their working capacity, are subjected to plastic deformation and necking before final failure. Therefore, testing with loads beneath the F_y alone is insufficient to describe the behaviour of grouted rock bolts on site. According to the tests conducted by Li et al. (2016b), the ultimate load to pull out the bolt increases linearly with an increase in the embedment length of the bolt until a certain limit. In the case shown in Fig. 1 this is at about 23 cm; which seems to coincide with the F_y of the bolt. After that, the increase slows down until the load reaches the ultimate tensile strength (F_u) of the bolt, at which point the bolt bar ruptures. The bolt bar is subjected to elastic deformation in the linear portion of the curve, implying a constant bond strength, while the non-linear portion of the curve may be associated with plastic deformation of the bolt steel and a change in the bond strength. The pull-out strength is dependent on many factors, such as the steel properties, grout properties, including the aggregate size and curing conditions and steel surface (e.g., corrosion protection).

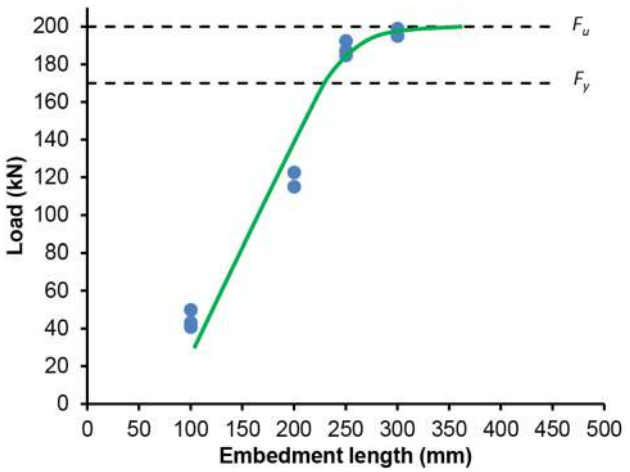

Fig. 1 The pull-out load versus embedment length of grouted rebar bolts 20 mm in diameter (Li et al. 2016b)

In this paper, the contribution of the plastic deformation of the bolt steel to the bolt-grout bond is investigated. The main objective is to present a theory, and supporting test data, for the mechanics of grouted rebar bolts subjected to pull forces, with a special focus on bolts pulled with forces above the steel F_y. Also presented are the equations used to calculate the critical embedment length of rock bolts subjected to such loads.

2 Theoretical Background

To understand the pull-out behaviour of a rock bolt, it is important to understand the average bond shear strength between the grout and bolt, which is defined by

$$\tau = \frac{F}{\pi d_b (L - S)} \tag{1}$$

where τ is the average shear strength, F the applied load, L the embedment length, S the bolt displacement and d_b the bolt diameter.

The main factors influencing bond shear strength are the surface condition of the bolt and the strength of the grout (Yeih et al. 1997; Kılıc et al. 2002). The cylindrical surface of a rock bolt may be smooth, but it often has ribs or threads, where the size and pattern of which significantly affect bond shear strength. The strength of the grout is dependent on the ingredients used (amount and type of cement, silica, etc.) and the water/cementitious binder (w/c) ratio. More water, i.e., higher w/c values, results in less strength. Strength increases with time, and most of a bolt's strength is attained after about 7 days. Final strength is usually thought to be achieved after 28 days of curing.

For a bolt loaded beneath its F_y, Benmokrane et al. (1995) suggested a tri-linear bond slip model, as shown in Fig. 2. The y-axis is the shear stress on the bolt and the x-axis is the pull displacement. The peak stress is the bond shear strength, expressed by Eq. (1). The three different stages of the model are characterised as follows: in stage I, the bond shear stress increases linearly with the pull displacement;

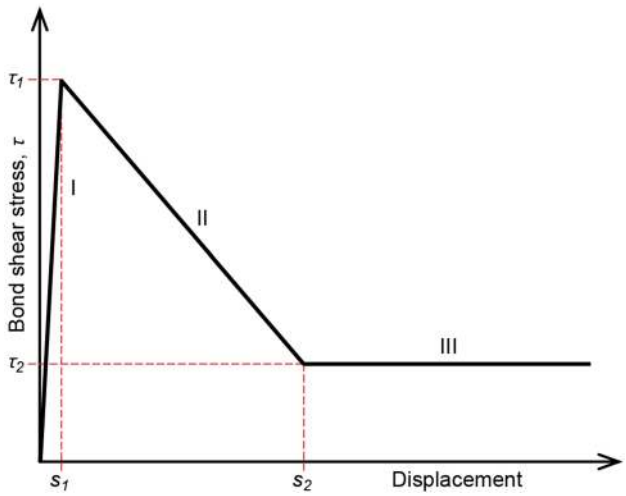

Fig. 2 Idealised trilinear bond slip model, based on Benmokrane et al. (1995)

in the transition between stage I and stage II, the debonding starts; in stage II, the debonding develops with decrement of the bond strength; finally, in stage III, a residual constant frictional resistance occurs. This approach seems to fit quite well with the results described by Li et al. (2016b). However, the model seems valid only for cases in which slippage occurs in the elastic state of bolt deformation and it is not applicable to cases in which the bolt bar yields before slippage occurs.

In a less simplified description, Yeih et al. (1997) presented a three-stage model (see Fig. 3) that was slightly different from the tri-linear model. In stage 1, there is a linear load displacement relationship, and the authors state that no debonding seems to take place. In stage 2, the curve starts to bend over, and debonding begins; shortly after, it reaches a maximum load value. Stage 3 is represented by the descending curve, which indicates decreasing bond strength. The angle of the curve in stage 3 and the length at which it turns (i.e., in the transition from stage 2 to 3) are based on a reduced confinement that features faster load reduction.

The shear stress along bolts has been discussed in several papers, including by Li and Stillborg (1999), Ren et al. (2010) and Blanco Martín et al. (2013); it has also recently been demonstrated experimentally with fibre optic cables by Vlachopoulos et al. (2018) and Forbes et al. (2020). Generally, the activated shear strength due to loading is higher closer to the collar of the hole than it is further inward. This applies especially to longer bolt segments. In the case of a short bolt at pull-out below F_y, the shear strength is at its highest at the outer end and is zero at the far end (Li et al. (2016a) and Vlachopoulos et al. (2018)). Even if the shear stress distribution along the bolt is not uniform at the time of being pulled out, it may be applicable to use an average shear strength as a simplified measure, since the total load carried by the segment will be the same.

The failure pattern of a grouted rebar bolt under a pull load is illustrated in Fig. 4, which shows that the failure surface in the grout is parallel to the bar and occurs at the top of the ribs (Bigaj-van Vliet 1999; Federation Internationale du Beton 2000). This type of failure was also observed by Gaztelumendi (2012). Numerical simulations conducted by Bulck (2015) showed that the debonding and fracturing of the grout begin almost simultaneously in the full length of the embedment when the final failure mode is slippage and no yielding occurs in the bolt bar. Yeih et al. (1997) proposed a similar failure pattern in their work: as stated above,

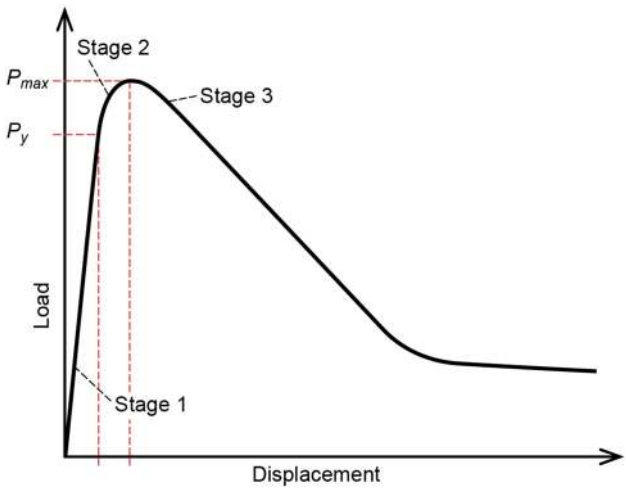

Fig. 3 Load–displacement curve of grouted bolt under pull load, based on Yeih et al. (1997)

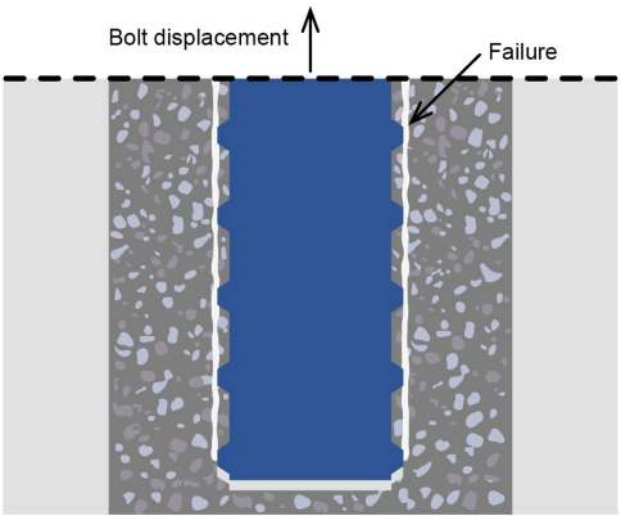

Fig. 4 Failure pattern of a rebar pull-out in the grout/bar-interface; redrawn based on Bigaj-van Vliet (1999) and Federation Internationale du Beton (2000)

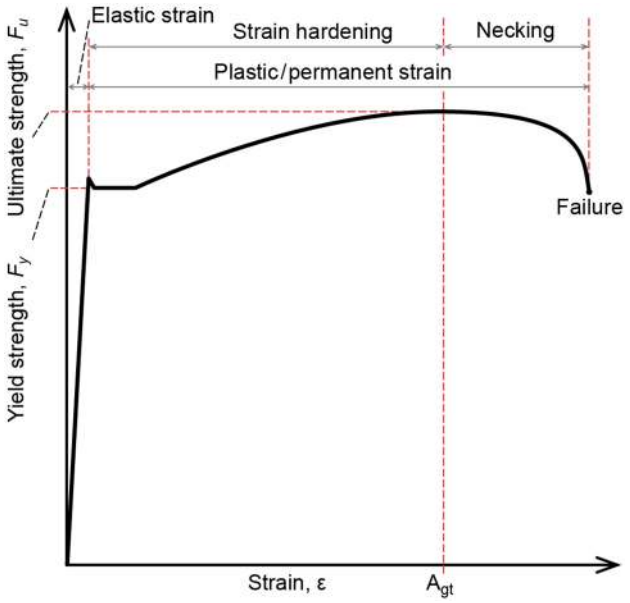

Fig. 5 Definition of terms and phases of steel deformation

they found that the debonding occurs in stage 2 when the pull-out curve starts to bend over.

Besidesto F_y, special attention should be paid to two features of the steel: its plastic strain and its strain hardening. Figure 5 shows a typical stress–strain curve for the steel used in rebar bolts. The strain is very small before the load reaches F_y. This is the elastic strain that will be reversed when the bolt is unloaded. When the load is beyond F_y, the bolt is subjected to plastic deformation. The elongation strain in this phase contains a component that will not be reversed when the load is reduced, that is, a permanent plastic strain. Plastic strain increases the strength of the steel until the load reaches F_u. This phenomenon is called *strain hardening*. During strain hardening, the strain is uniform across the whole length of the bolt. Necking starts after the load reaches F_u and ends with the rupture of the bar. The strain at F_u, denoted as A_{gt}, represents the maximum strain before necking starts. Generally, A_{gt} is correlated with the strength of the steel, in that stronger steels have lower A_{gt} values. A small radial contraction also occurs in the bolt as a result of the Poisson effect.

3 Pull-Out Tests of Rock Bolts

The pull-out tests reported in this paper are follow-up tests to those reported by Li et al. (2016b). The results of strain gauge measurements on the bolts in some of the follow-up tests were briefly reported by Li et al. (2016a) and are not included in this paper.

Fig. 6 The rebar bolt used in these tests: 20 mm in diameter, made of type B500NC steel and corrosion protected with hot galvanising and powder coating

3.1 Materials and Equipment

Three series of pull-out tests were performed in this study: A, B and S. The bolts in series A were grouted in holes percussively drilled in a 1 m^3 concrete block with a spacing of 17 cm. The bolts in series B and S were grouted in steel tubes and had markings for measuring plastic deformation. In addition to markings, the bolts in series S had strain gauges on the bolt surface for the measurement of the axial load during testing.

3.1.1 Type of Rock Bolt

The rock bolt used in the tests was a 20 mm diameter rebar bolt made of type B500NC steel, which is often used for rock support in tunnels in Norway. The quality of the bolt was according to NS 3576–3 standard (Standard Norge 2012). B500NC has a characteristic F_y and F_u of 157 and 188 kN, respectively, a characteristic A_{gt} of 8% and a rib pattern as shown in Fig. 6. However, both the strength and ductility of the bolt samples in the tests were higher than their characteristic values. The bolt steel had been treated with a double corrosion protection of hot galvanizing and powder coating.

3.1.2 Grout and w/c Ratio

The cement used in the tests was Zinckbolt, manufactured by Mapei, which is specifically made for the grouting of rock bolts. Refer to Li et al. (2016b) for the calculation of the w/c ratio of the grout for bolt installation in the tests.

The uniaxial compressive strength (UCS) of the grout was determined by testing cubic specimens that were 100 × 100 × 100 mm in size (Li et al. 2016b). Three specimens were tested for each w/c ratio (i.e., 0.4, 0.5 and 0.6).

3.1.3 Test Specimens

The embedment lengths and w/c ratios were selected based on previous tests, toget the different types of pull-out

mechanisms described later. Twenty bolts were tested across the three series, with ten bolts in series A, four in series B and six in series S. More detail about embedment lengths and w/c ratios is given in Sect. 4.

The 10 bolts in series B and S had markings to allow for the measurement of permanent strain, while the six bolts in series S also had strain gauges for load measurement. The strain gauge measurements are not discussed in this paper, because the range of the strain gauges is not large enough to measure plastic deformation. It should be noted that installation of the strain gauges required a groove along the bolt length in series S bolts, resulting in a smaller cross-section and, thus, a slightly lower F_y in these bolts. The cross-section area of the bolts in series S was 297 mm^2, compared to 316 mm^2 for the bolts in series A and B.

3.1.4 Bolt Holes

For series A, 48 mm diameter holes were percussively drilled in a large concrete block with a UCS of approximately 110 MPa, to mimic in-situ conditions. For series B and S, steel tubes with inner/outer diameters of 46.5/66.5 mm were used. The tubes were spiral cut shallowly inside to increase friction. Steel tubes were used to allow the bolts to be retrieved after testing, so that they could be cut open to measure plastic deformation.

3.1.5 Measurement of Plastic Bolt Deformation

Small grooves (or marks) were made on the longitudinal rib of the bolts using a grinder. The grooves were nominally spaced 10 mm apart, with a total of 30 segments being made between the grooves, marked S_1–S_{30} (Fig. 7). The length of each segment was measured before (l_0) and after (l_1) testing using a digital sliding calliper, and the plastic strain for each segment was calculated based on the elongation of the segment after testing. The strain (s) was calculated using the formula $s = (l_1 - l_0)/l_0$.

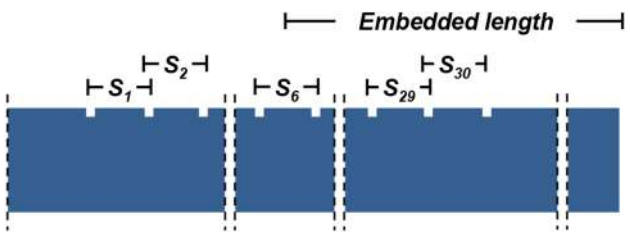

Fig. 7 Marks on the longitudinal rib (see Fig. 5) used to measure plastic deformation

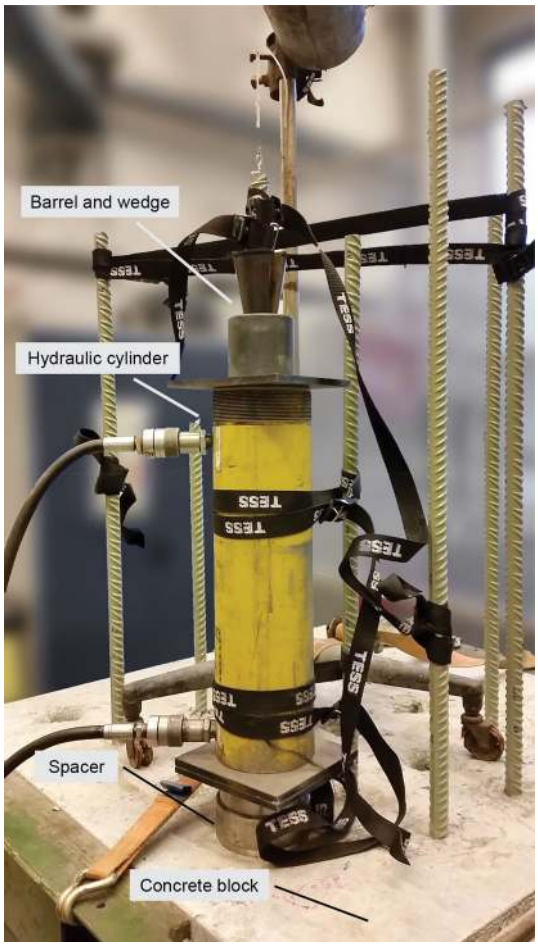

Fig. 8 Test setup for series A bolts grouted in a concrete block

3.2 Test Setup

A hydraulic jack was used to load the bolts. The arrangements for series A and series B/S can be seen in Fig. 8, Fig. 9. The free length of the bolt included both the length of the jack (420 mm) and the spacers; in total, it was approximately 600 mm. At the yield load, the (elastic) elongation of the free length was approximately 1.5 mm. For each percentage point of yielding strain, approximately 6 mm of the displacement presented in the figures was the result of deformation of the free length.

For series A bolts, the base for the extensometer rested on the concrete block, while for series B and S bolts, the extensometer was fixed on the jack. The bolt was fixed to the jack using a barrel and wedge fastener. A spacer was used between the block/steel tube and the jack to let the bolt form a cone where it exited the grout. Allowing the formation of such a cone is important for simulating scenarios such as the widening of a joint.

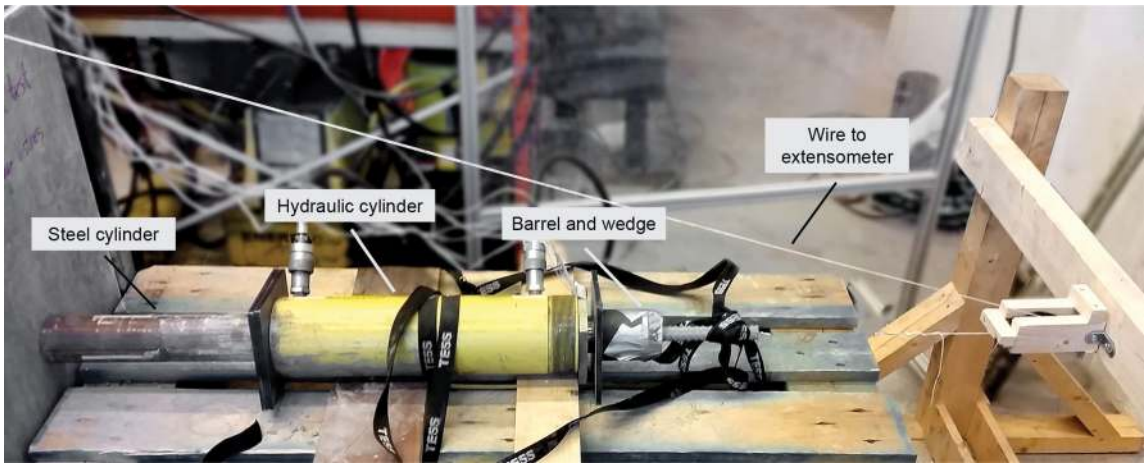

Fig. 9 Test setup for series B and S bolts, grouted in a steel tube (outer/inner diameters = 66.5/46.5 mm)

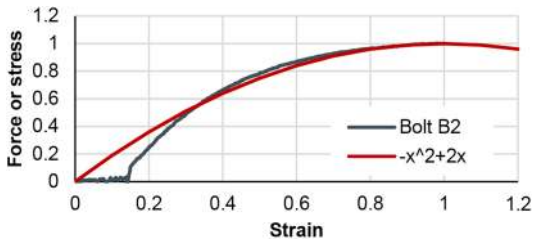

Fig. 10 Approximation of the stress–strain relationship

3.3 Bolt Strain-to-Stress Estimation and Shear Stress Calculation

By looking at plastic strain, which was measured using the marks on each bolt, one can assess the stress that a bolt segment was subjected to by the end of the pull-out test. This stress can then be used to assess the shear stress (or residual strength) on the bolt segment and force loss along the bolt. To perform these calculations, an estimation was used, as described below.

The stress–strain (or force-strain) relationship, as shown in (2), is nonlinear in the strain hardening interval. To simplify the strain-to-stress calculation, an approximation was developed.

In Fig. 10, one can see the normalised stress–strain data for bolt B2. The left limit (maximum elastic strain and F_y) corresponds to coordinates 0,0, and the right limit (F_u and A_{gt}) to coordinates 1,1. Also plotted is the approximation

$$y = -x^2 + 2x \tag{2}$$

As seen in the plot, the approximation results in a slightly larger stress or force value at smaller strains, but it fits very well in cases of larger strains. The correlation between the two variables was $R^2 = 0.99$, in the range 0 to 1 for (normalised) strain (calculated using SPSS (IBM Corp. 2016)).

By inserting A_{gt}, F_y and F_u for a given steel type, the force in the plastic state of the steel can be calculated using the strain, as shown in Eq. (3). The elastic strain, which is very small compared to the A_{gt} and is estimated at zero, was left out to keep the equation simple. In the case of the specimens in this study, the bolts were unloaded to zero at the time of measurement so that elastic strain did not have to be considered. The bolt stress can then be calculated using Eq. (4).

$$F(s) = \left(-\left(\frac{s}{A_{gt}}\right)^2 + 2\left(\frac{s}{A_{gt}}\right) \right) \cdot \left(F_u - F_y\right) + F_y \tag{3}$$

$$\sigma(s) = \frac{4 \cdot F(s)}{\pi \cdot d_b^2} \tag{4}$$

where $F(s)$ is the force at a given strain, A_{gt} is strain at the ultimate force, $\sigma(s)$ is the stress at a given strain, F_y is the yield force and F_u is the ultimate force.

The shear stress for a segment can be calculated using the change in either the stress or the force. Derived from Eq. (5), and using force, this would equate to

$$\tau = \frac{F(s_e) - F(s_s)}{d_b \cdot \pi \cdot L_S} \tag{5}$$

where $F(s_s)$ is the force at the start of a segment, $F(s_e)$ the force at the end of a segment and L_S the segment length.

When the length of the embedded bolt plastic deformation zone and the maximum strain are known, as in this case, one can use these values to calculate bolt stress at different positions along the bolt. In the equation below (Eq. (6)), the

position $x=0$ is at the elastic/plastic transition, with increasingly positive values outward from the bottom of the hole. Presuming a linear distribution of the strain, this will be

$$\sigma(x) = \left(-\left(x \cdot \frac{(s_m/L_P)}{A_{gt}} \right)^2 + 2\left(x \cdot \frac{(s_m/L_P)}{A_{gt}} \right) \right) \cdot (\sigma_u - \sigma_y) + \sigma_y [0, L_p] \quad (6)$$

where $\sigma(x)$ is the stress at position x in the plastic embedded zone, s_m the maximum bolt strain in the embedded zone, L_P the plastic embedment length, σ_y the yield stress and σ_u the ultimate yield stress.

Using N (not kN) for force and mm for length, the stress is given in MPa for these equations. Strain and A_{gt} are divided by each other, and so the same proportions need to be used.

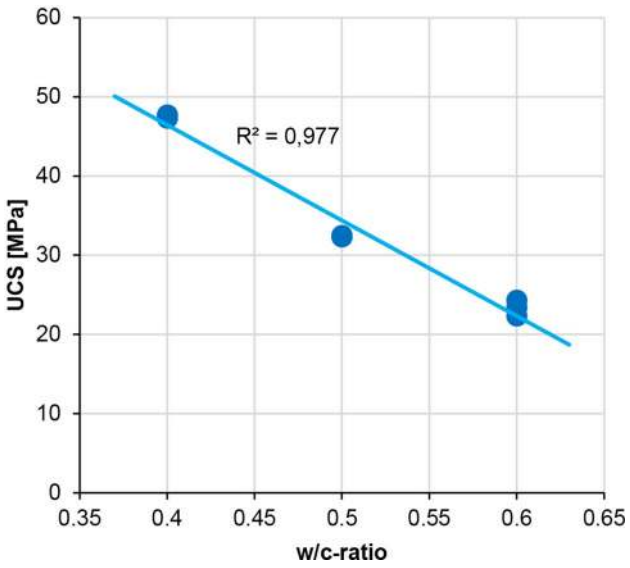

Fig. 11 Correlation between grout strength and w/c ratio

4 Results

4.1 Specimen Overview

An overview of the testing conditions (i.e., the embedded length, w/c ratio and curing time) and the maximum load and failure mode are presented in Table 1. It is worth noting that there was an extended curing time for bolts B3 and B4, which may have resulted in higher grout strengths. The relationship between grout strength and w/c ratio is presented in Fig. 11. The curing time of the grout cube specimens was 7 days for w/c 0.4 and 0.6 and 9 days for w/c 0.5.

4.2 Pull-Out Rests

Figure 12 shows the load–displacement curves for series A bolts, which indicate that bolts A1–A4 were pulled out

Table 1 An overview of bolt specimen testing conditions, alongside maximum load and failure mode data

Specimen	Embedded length [mm]	w/c ratio	Grout curing time [days]	Max load [kN]	Failure mode
S1	600	0.4	10	190	Terminated at start of necking
S2	600	0.4	10	191	Terminated at start of necking
B1	300	0.4	10	203	Terminated at start of necking
B2	300	0.4	10	203	Terminated at start of necking
B3	300	0.5	12	198	Slip failure
B4	300	0.5	12	198	Slip failure
S4	450	0.6	10	184	Slip failure
S6	450	0.6	10	184	Slip failure
S3	300	0.6	10	170	Slip failure
S5	300	0.6	10	172	Slip failure
A1	100	0.4	7	103	Slip failure
A2	100	0.4	7	98	Slip failure
A3	150	0.4	7	155	Slip failure
A4	150	0.4	7	163	Slip failure
A5	200	0.5	9	175	Slip failure
A6	200	0.5	9	178	Slip failure
A7	300	0.5	9	199	Terminated at start of necking
A8	300	0.5	9	198	Terminated at start of necking
A9	450	0.5	9	193	Terminated at start of necking
A10	450	0.5	9	201	Terminated at start of necking

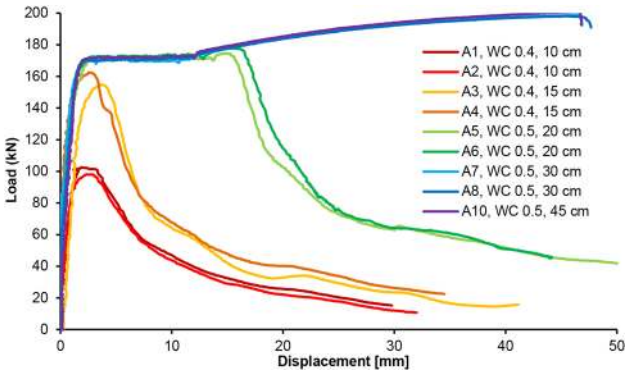

Fig. 12 Load-deformation curves for series A bolts

with a force lower than the F_y of the bolt steel. Bolts A5 and A6 were pulled to a load higher than the F_y of the steel before they slipped in the grout/bolt interface. Bolts A7, A8 and A10 were pulled to F_u without being pulled out of the hole. The three different modes of failure mentioned above correspond to the different pull-out mechanisms that are defined in Sect. 5.1. For bolt A9, there was an error in the data recording device and unfortunately there are no data to present.

Bolts B1, B2, S1 and S2 were pulled to F_u and terminated manually at the start of necking. The load–displacement curves for these bolts are presented in Fig. 13. The F_y and F_u of the S bolts were lower than those of the B bolts because the cross-section area of the S bolts was smaller, as mentioned above. The test results of the rest of the B and S bolts are presented in Fig. 14. All specimens slipped in the bolt-grout interface during the strain hardening stage.

4.3 Measurement of Plastic Deformation

Permanent plastic deformation, or plastic strain, was measured using the marks on the bolts, as described in Sect. 3.1.5. The measured strains along bolts B1, B2, S1 and S2 are presented in Fig. 15, the loading curves of which are shown in Fig. 13. Zero on the *x*-axis is the starting position of the initial embedment of the bolt. During the test, a cone of grout was pulled out so that the essential embedment started a few centimetres to the right of the zero position. It was observed that the strain of bolts B1 and B2 was only slightly reduced at the 3–4 cm position compared to the strain in the free length (− 5 to 0). The strain peaks in the S bolts at − 5 cm and 0 cm are due to the necking of the bolt bars.

The measured strains along bolts B3, B4, as well as the rest of the S bolts, are presented in Fig. 16. The loading curves for these bolts are shown in Fig. 14. All bolts were loaded to levels in the stage of strain hardening and were pulled out of the holes with slippage. Similarly, the plastic strain remained constant in the free length and was slightly reduced when the embedment depth was approximately 5 cm due to fracturing in the grout.

The load in the free length of the bolt is equal to the applied load, and the strain is theoretically constant. In intervals where a reduction in strain occurs (e.g., 3 to 15 cm for B1), it can be assumed that the load in the bar reduces from the maximum load and reaches F_y at the point where the strain is zero. In the case of the bolt with zero plastic strain and a load below F_y, other research (Li et al. 2016a; Vlachopoulos et al. 2018) has shown that the bolt load reduces inward along the bolt due to the shear strength in the bolt-grout interface.

5 Behaviour of Grouted Rebar Bolts Under Pull Load

This section puts forward a theory regarding the loading process of grouted rebar bolts under pull and proposes a method for estimating the critical embedment length of a bolt. It also verifies the theory using the results presented above.

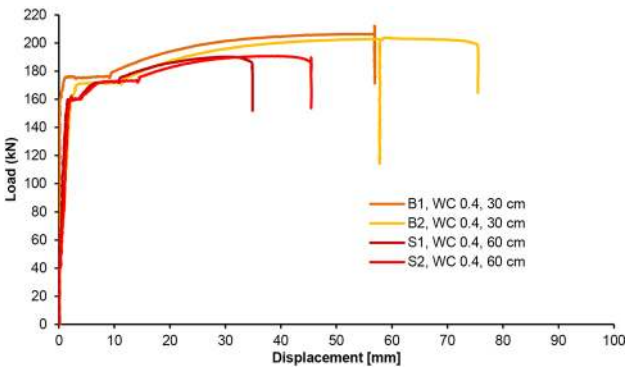

Fig. 13 Load–displacement curves for the series B and S bolts which were pulled the start of necking

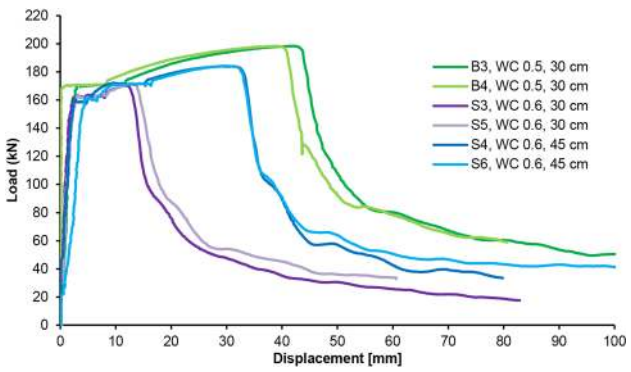

Fig. 14 Load–displacement curves for the series B and S bolts which were pulled out at a force higher than the *F*y of the bolt steel

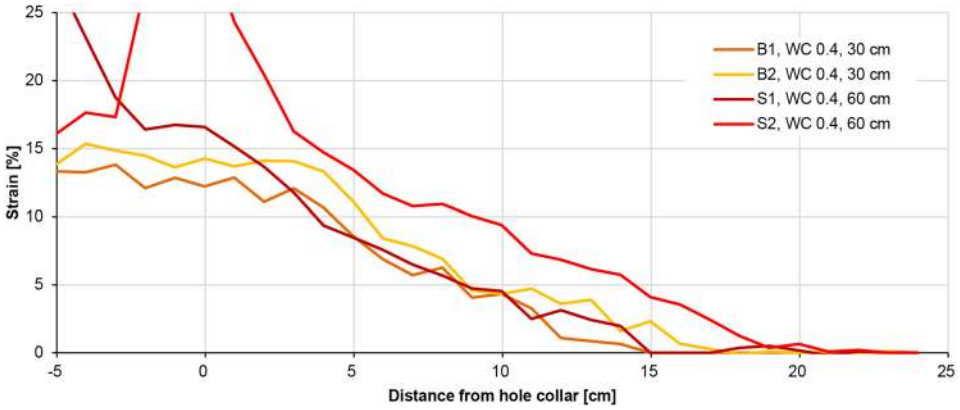

Fig. 15 Axial strain measured along the bolts with a w/c ratio of 0.4; note that bolt embedment is longer than what is shown in the figure

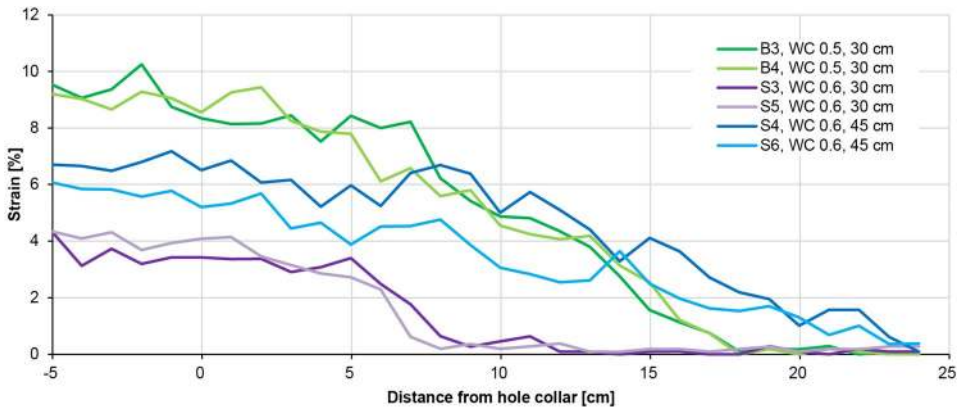

Fig. 16 Axial strain measured along the bolts with w/c ratios of 0.5 and 0.6; note that the bolt embedment is longer than what is shown in the figure

5.1 Pull-Out Mechanisms

Based on the test results reported by Li et al. (2016b) and the tests conducted in this study, the behaviour of grouted rebar bolts under pull loads can be classified into three types:

Type 1: Pull-out slippage occurs when the applied load is less than the yield load of the bolt bar. The bolt steel is subjected to elastic deformation during loading, and shear failure occurs in the bolt-grout interface of the entire embedment length.

Type 2: Pull-out slippage occurs when the applied load is above the yield load of the bolt bar. The bolt steel is subjected to both elastic and plastic deformation during loading, and shear failure occurs in the bolt-grout interface of the entire embedment length.

Type 3: Failure of the bolt bar occurs when the bolt bar necks and ruptures. The bolt steel is subjected to both elastic and plastic deformation in its embedded length. In the embedment length of plastic deformation, sufficient residual shear strength in the bolt-grout interface builds up during deformation preventing pull-out.

5.1.1 Type 1: Pull-Out Slippage Below Bolt Bar Yield Load

The behaviour of this type conforms well to the tri-linear model proposed by Benmokrane et al. (1995) and the curve presented by Yeih et al. (1997).

The load-deformation curve of bolts with the type 1 pull-out mechanism can be divided into three stages, referred to as stages 1, 2 and 3 in Fig. 17. In stage 1, the load increases until it reaches its maximum value, at which point the failure cone forms in the collar of the grout-filled hole (Fig. 18a). This results in a reduction in the embedded length. The load–displacement correlation is linear at the beginning, until the formation of the failure cone starts. At peak load, the failure cone is detached from the grout in the hole, and shear failure is mobilised along the bolt-grout interface (Fig. 18b). The curve in Fig. 17 indicates that total displacement of the bolt is approximately 3 mm; total displacement is the sum of the elastic elongation of the free length of the bolt and the displacement of the embedment length. Elastic displacement is approximately 1 mm at a load of 100 kN. Therefore, the movement of the embedment length contributes to approximately 2 mm of the total displacement. After the peak, the load decreases rapidly, corresponding to more failures in the bolt-grout interface, marked as stage 2 on the curve in Fig. 17. The load decrease decelerates and enters

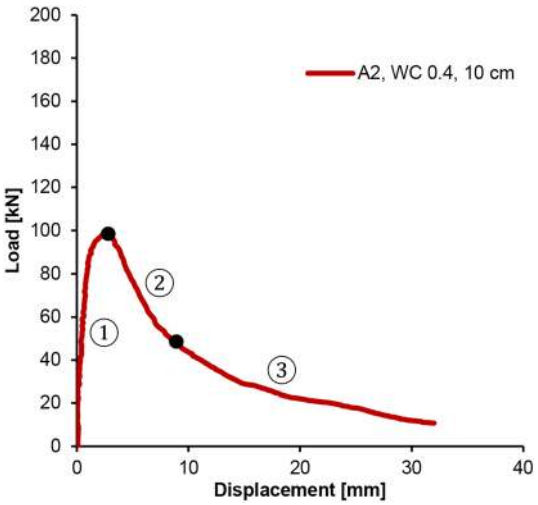

Fig. 17 A typical load–displacement curve for a pull-out bolt that underwent the Type 1 pull-out mechanism

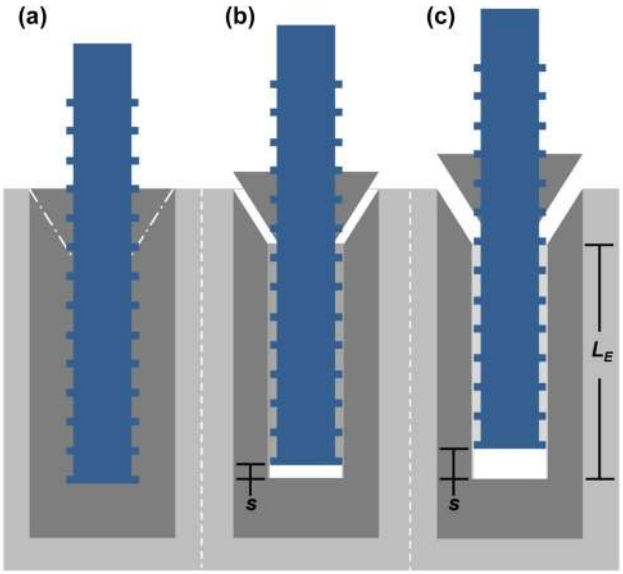

Fig. 18 The behaviour of bolts according to loading conditions for the Type 1 failure mechanism: **a** in stage 1, **b** in stage 2 and **c** in stage 3; L_E is the elastic embedment length

stage 3 after the fractures between the ribs coalesce, as illustrated in Fig. 18c. The turning point between stages 2 and 3 is hard to determine in practice.

Figure 17 indicates that the load apparently decreases with further displacement in stage 3. However, the effective embedment length decreases with slip during this stage. By taking into account the shortening of the embedment length, as seen in Eq. (1), the residual shear strength of the bolt-grout interface is approximately constant during stage 3.

5.1.2 Type 2: Pull-Out Slippage Above Yield Load

Type 2 failure occurs during the strain hardening stage, that is, at load levels between the F_y and the F_u of the bolt steel. Figure 19 shows a typical load–displacement curve for this failure type. The deformation and failure process of the bolt can be divided into five stages, as shown in the figure. The states of the bolt during those stages are sketched out in Fig. 20, where the lighter colour indicates bolt steel undergoing plastic deformation.

Stage 1 starts at the beginning of loading and lasts until the F_y of the bolt steel is reached (see Fig. 19). The bolt only undergoes elastic deformation during this period (Fig. 20a). In stage 2, the free length of the bolt yields, with an increase in displacement, but the load remains at the F_y level. The failure cone may be formed at the end of stage 2 (Fig. 20b). Stage 3 starts when the load increases with strain again, marking the beginning of strain hardening. The yielding of the steel propagates into the embedded segment of the bolt, and at the same time, debonding starts and propagates along the bolt-grout interface, with an increase in the load (Fig. 20c). The partially debonded segment of the embedded length is marked L_P and called the plastic embedment length, while the rest of the embedded length is in the elastic deformation stage and thus called the elastic embedment length.

The relative movement of the ribs is larger at positions closer to the opening of the hole than it is further inside the hole. As seen in the results from Type 1 failures, the ribs that have moved exhibit a lower shear strength than those that have not moved. It is therefore reasonable to assume that shear strength is not constant in the L_P and that it in fact decreases closer to the hole opening. The bolt steel is simply yielding without hardening in the front of the plastic propagation, which may make it easier to exceed peak bond strength at the deformation front, in turn enabling easier propagation. Failure of the bolt-grout interface may result in the dilation of broken grout material, which can lead to an increase in normal stress on the interface. However, the radial contraction of the bolt that occurs as a result of the steel yielding could reduce normal stress on the interface and result in a reduction in residual shear strength.

In stage 3, if one assumes that the elastic embedment length still carries the load below the F_y after the bolt bar starts to deform plastically, then the load increment beyond the yield load ($F_u - F_y$) is purely borne by the L_P. The elastic embedment length (L_E) becomes shorter as the plastic deformation front propagates into the hole with increasing load. Finally, the critical elastic embedment length (L_{CE}) is reached when the pull load is at its highest (Fig. 20d). Then stage 4 starts, and the entire embedment length of the bolt slides in the grout (Fig. 20e). The behaviour of the bolt in stage 5 is similar to stage 3 of Type 1.

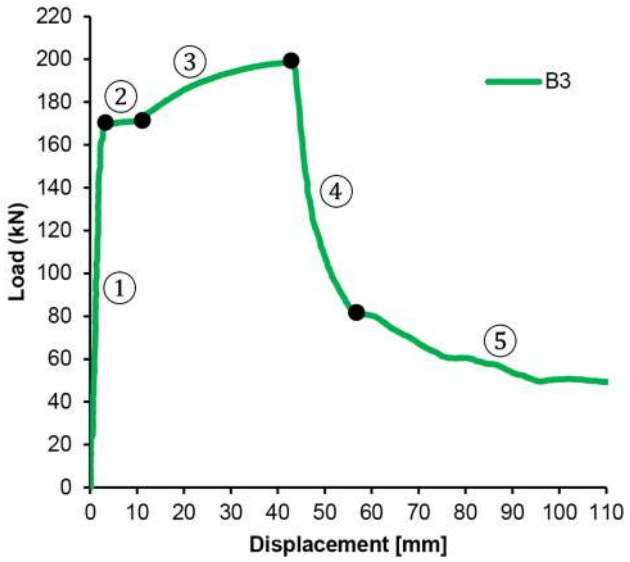

Fig. 19 A typical load–displacement curve for a pull-out bolt that underwent the Type 2 pull-out failure mechanism

The yield load of the bolt shown in Fig. 19 was 171 kN, while the slip occurred at 198 kN. Given the assumption above that the maximum elastic load, i.e., the yield load, is equal to the total load on the L_E, the load on the L_{CE} was 171 kN when slip started. Therefore, the residual load on the plastic length was 198 – 171 = 27 kN.

5.1.3 Type 3: Rupture of the Bolt Bar

Type 3 failure demonstrates the same behaviours as Type 2 failure in its first three stages, but at the end of stage 3, failure occurs in the bolt bar instead of in the bolt-grout interface. Figure 21 shows a typical load–displacement curve for such a failure, while Fig. 22 outlines the state of the bolt during the test. When comparing Type 2 failure specimen B3 (Fig. 19) with Type 3 failure specimen B2 (Fig. 21), the embedment length is the same, but the w/c ratio of the grout is lower in Type 3, resulting in a higher grout strength.

In stage 3, the plastic deformation of the bolt bar propagates inward into the hole, with increments of the pull load

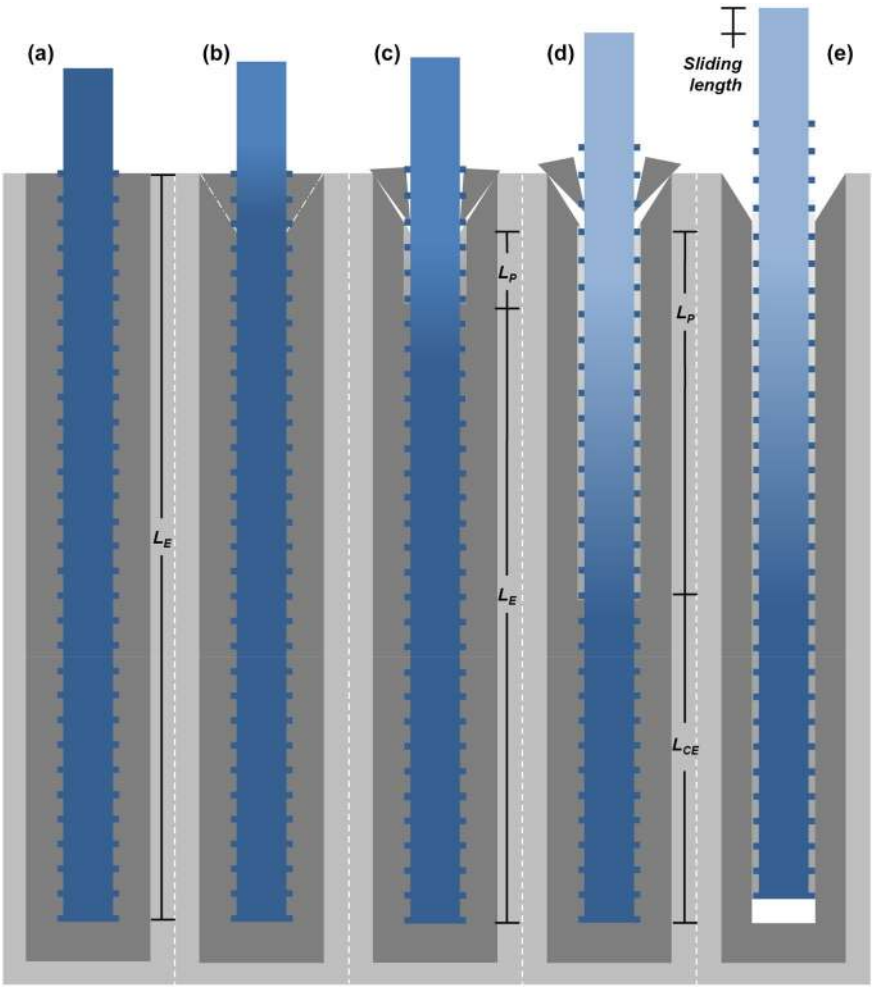

Fig. 20 The behaviour of the bolt in different loading conditions for the Type 2 failure mechanism: **a**–**c** correspond to stages 1, 2 and 3, respectively; **d** is at the point of failure between stages 3 and 4; and **e** corresponds to stage 4

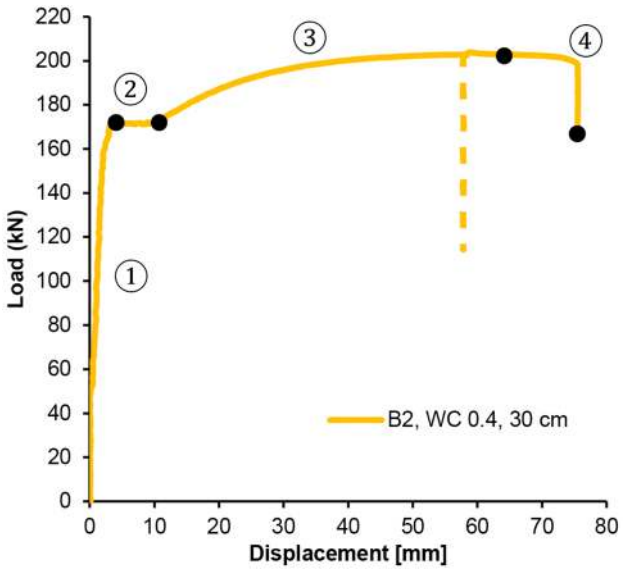

Fig. 21 A typical load–displacement curve for a rock bolt that underwent the Type 3 failure mechanism; the embedment length is 300 mm and the w/c ratio is 0.4; the circled numbers indicate stages; the stapled line reflects data gathered due to equipment error

(Fig. 22c). The L_P increases while the L_E decreases during this process. When the L_P increases to a length where the total shear load is equal to $F_u - F_y$, the bolts starts to neck, as its A_{gt} is reached. That length is the L_{CP} (Fig. 22d). Further pull displacement causes the necking to progress and results in the rupture of the bar (Fig. 22e).

For the loads shown inFig. 21, the F_y of the bolt bar was 171 kN, while the F_u was 203 kN. The L_E managed the 171 kN, while the L_P increased until the shear load on the plastic segment of the embedded length reached 32 kN.

To avoid slippage, the total embedment length of the bolt (L_{CT}) must be longer than the sum of the cone length, the L_{CE} and the L_{CP}.

5.2 Pull-Out Model

As mentioned above, there are two critical embedment lengths for the pull-out of a grouted rebar bolt: one related to the embedded portion of the bar, which experiences elastic steel deformation; and one related to the embedded portion of the bar, which undergoes plastic steel deformation. The load below F_y is restrained by the elastic embedment length

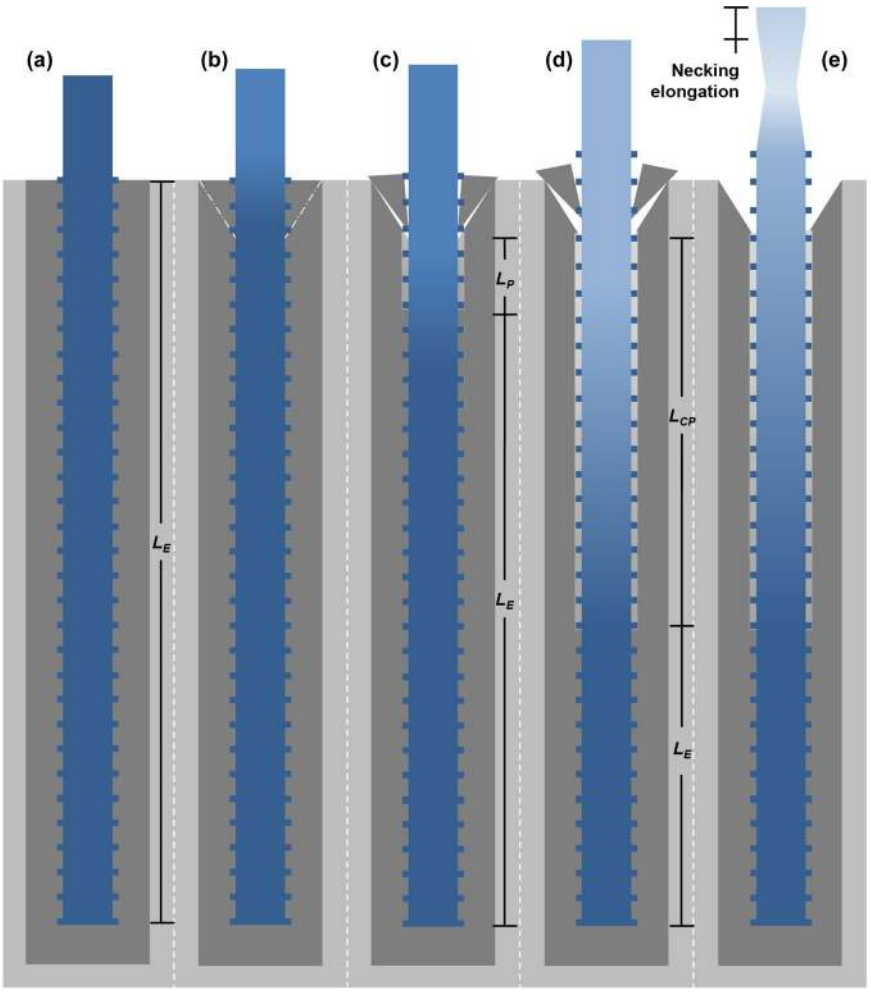

Fig. 22 The behaviour of the bolt in different loading conditions for the Type 3 failure mechanism; **a**–**c** correspond to stages 1, 2 and 3, respectively; **d** is at the point of failure between stages 3 and 4; **e** corresponds to stage 4

due to the bond between the bar and the grout, which is mainly dependent upon the mechanical strength of the grout, the rib geometry and the chemical bar-grout bond. The load above F_y (i.e., $F_u - F_y$) is restrained by the length undergone plastic steel deformation. During onloading, the plastic length develops until the total residual strength of the failed bar-grout bond in the plastic length is greater than $F_u - F_y$.

5.2.1 Elastic Limit

A 200 mm-long bolt segment elongates by 0.25 mm when it is subjected to a pull load at the yield limit. This is a very small deformation and, therefore, the bond shear stress on such a segment embedded in concrete is constant along the length of the segment when debonded and can be calculated using Eq. (1). This results in zero stress at the bolt's far end and a stress corresponding to the applied load at the other end. Laboratory tests by Li et al. (2016a) and Vlachopoulos et al. (2018) using strain gauges and fibre optic cables, respectively, demonstrated the effects of a stress distribution of this type on embedment length. As shear stress is constant along the elastic length, it follows that failure happens along the entire length at once, as shown by Bulck (2015).

Being derived from Eq. (1), the L_{CE} is expressed as

$$L_{CE} = \frac{F_y}{\tau_m \cdot \pi \cdot d_b} \tag{7}$$

where L_{CE} is the critical elastic embedment length, F_y the steel yield load and τ_m the average maximum bond shear strength.

5.2.2 Plastic Limit

It was assumed that bond shear strength on the bolt segment that had undergone plastic bolt deformation was distributed as shown in Fig. 1, with a maximum residual strength at the plastic-elastic boundary and a minimum residual strength at the bottom of the cone crater. The decrease in residual shear strength towards the hole collar may be attributed to two factors: the severe crushing of the grout owing to the significant movement of the bolt bar; and the contraction of the bolt in a radial direction. These two factors result in reduced friction and normal stresses on the bolt-grout interface and, thus, reduced shear stresses.

From a material point of view, the L_{CP} is believed to be dependent on the deformability of the steel (A_{gt}), the surface profile of the bolt and the strength of the grout, the latter two being represented in the shear strength of the bolt-grout bond. The consequence of this is that the L_{CP} is short for stiff steel (i.e., steel with a low A_{gt}) and long for soft steel (i.e., steel with a high A_{gt}), because stiff steel will deform less than soft steel both axially and radially. For example, if steel A_{gt} is zero, there will be no plastic deformation and, hence, no movement in the grout, giving a propagating plastic length. At the other theoretical extreme, if the A_{gt} is very high, the minimum residual shear strength at the hole collar may become zero, resulting in a case were the residual strength never reaches the needed strength and propagation continues down the hole until pull-out. This may be a fourth type of pull-out mechanism that was not documented by the tests conducted in the current study.

Assuming that the reduction is linear, the following relationship exists between the bond shear strength and the L_{CP}, according to Eq. (1):

$$\frac{\tau_{Rmsx} + \tau_{Rmin}}{2} = \frac{F_u - F_y}{\pi d_b L_{CP}} \tag{8}$$

or

$$L_{CP} = \frac{2\left(F_u - F_y\right)}{\pi d_b \left(\tau_{Rmax} + \tau_{Rmin}\right)} = \frac{F_u - F_y}{\pi d_b \tau_{Ra}} \tag{9}$$

where L_{CP} is critical plastic embedment length, F_u is the ultimate steel strength, τ_{Rmax} is the maximum residual shear strength, τ_{Rmin} is the minimum residual shear strength and τ_{Ra} is the average residual shear strength.

5.2.3 Cone Section

It is most likely that the cone section, or no bound length (L_{NB}), is mainly dependent on hole diameter and grout strength in the case of holes in rock masses of good quality. Furthermore, the cone angle may be dependent on grout strength and the depth may be related to hole diameter. The rock around the hole collar may be broken under the forces transferred from the bolt and grout, if the rock is very weak.

In addition to the actual cone depth, the L_{NB} may extend a small distance into the hole beyond the actual cone formation due to the crushing and spalling of the grout and the radial contraction of the steel.

5.2.4 Total Critical Embedment Length

For a grouted bolt that is subjected to a load at its F_u, the total critical embedment length of the bolts (L_{TC} in the equations below) is equal to the sum of the three lengths described above:

$$L_{TC} = L_{CE} + L_{CP} + L_{NB} \tag{10}$$

Or

$$L_{TC} = \frac{F_y}{\tau_m \pi d_b} + \frac{2\left(F_u - F_y\right)}{\pi d_b \left(\tau_{Rmax} + \tau_{Rmin}\right)} + L_{NB} \tag{11}$$

5.3 Verification of the Theory

Using the equations presented in Sect. 3.3 and the strain data presented in Fig. 15 and Fig. 16, the axial stress in the bolt steel and shear stress in the bolt-grout interface in the plastic zone can be estimated. The axial stress and shear stress for bolts B1, B2, B3 and B4 are presented in Fig. 24 and Fig. 25. Similar diagrams can be plotted for bolts S1–S6, but these are not presented in this article. In L_E, a simplified model of shear stress using an average value has been used to approximate this behaviour.

Looking at the solid lines in Fig. 24 and Fig. 25, which were calculated using the stress calculations from Eq. (6) in Sect. 3.3, we can see the development of shear strength assumed in our model from Fig. 23. It can also be seen that the shear stress derived from the strain measurements, titled 'Shear stress derived from bolt stress' in the figure legend, changes according to our theory's predictions. Notice that, in the graphs, an interval of 20 mm was used for each plotted point rather than the original 10 mm interval used in the calculations, to smooth the curves.

One key element of the theory is that the total shear load on the plastic deformation length is equal to the force increment for strain hardening, that is, $F_u - F_y$, and that the elastic embedment length carries the load below F_y. The force increment ($F_u - F_y$) and the values estimated using the measured strains and the equations in Sect. 3.3 are presented in Table 2 for all S and B bolts. The largest deviation between the calculations and measurements was found for bolts S3 and S5. These bolts had only three strain measurements available for calculation and, therefore, a greater degree of variation were expected. As expected, the results of the two calculation methods were similar, since the input values were based on the same measurements and estimations.

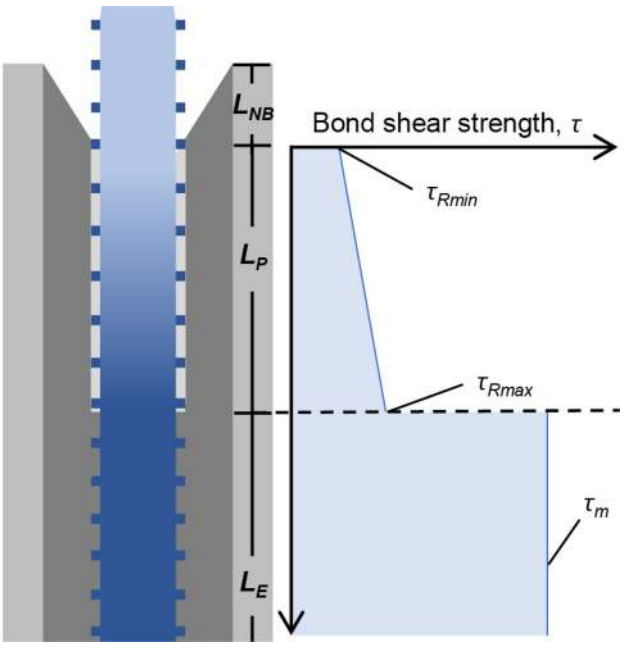

Fig. 23 A model for the distribution of bond shear strength along the embedment length of the bolt

5.4 Other Applications of the Theory

The loading condition used in bolt pull-out tests is, in principle, the same condition that occurs when rock bolts override a rock joint (or fracture) that widens along the length axis of the bolt. If the bolt bar fails, it does so in line with the Type 3 failure mode (i.e., no pull-out) described in this paper. For example, the bolts that underwent Type 3 failure during these tests (B1, B2, S1 and S2) showed a relative movement between the bolt steel and hole collar of approximately 10 mm. This would give a joint opening of approximately 20 mm before bolt failure, as the failure happens on both sides of the joint. For bolts with higher w/c ratios, the joint opening before bolt failure increases, as the plastic zone develops further.

6 Discussion

The tests reported on in this paper were designed to investigate the responses of a cement-grouted rock bolt subjected to a load higher than the F_y of the bolt steel. The results were used to examine the mechanics of the pull-out process and to assess the critical embedment length of the bolts.

Steel deformation at the F_u of the steel is outside the range of accurate deformation measurement methods, which use strain gauges and fibre optic cables. Instead a crude—but simple and cheap—method was used to record large plastic deformation in the bolt steel: the distance changes between marks on the bolt were measured using a digital

Table 2 $F_u - F_y$ values, based on test measurements and calculations

Specimen	F_y [kN]	F_u [kN]	F_u-F_y [kN]	Calc.[a] [kN]	Calc.[b] [kN
S1	159	190	31	29	30
S2	160	191	30	29	30
B1	175	206	31	31	31
B2	172	203	31	31	31
B3	171	198	28	29	29
B4	171	198	27	28	28
S4	158	184	26	22	22
S6	160	184	24	21	22
S3	161	170	9	14	14
S5	162	172	10	12	13

[a]Calculated using measured strain values

[b]Calculated using the theory presented in Sect. 3.3

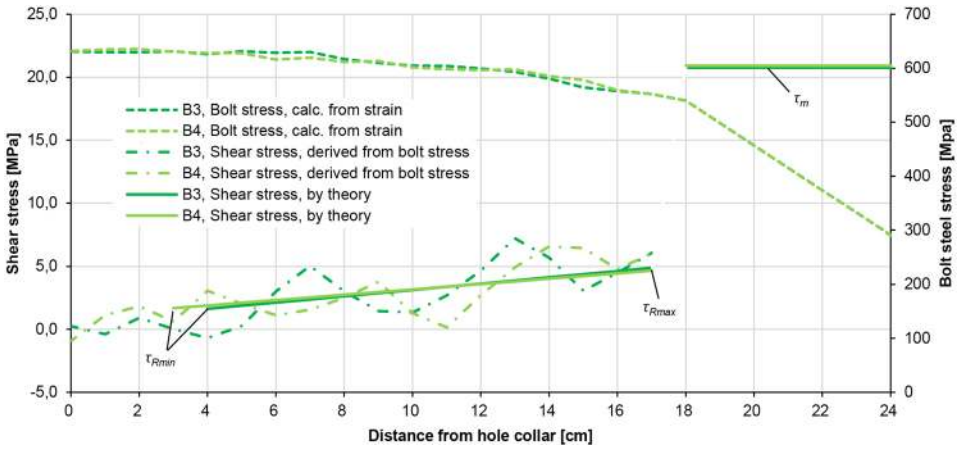

Fig. 24 Axial bolt stress and bond shear stress for Type 2 pull-out tests; these were calculated using measured plastic strain values and the equations presented in Sect. 3.3

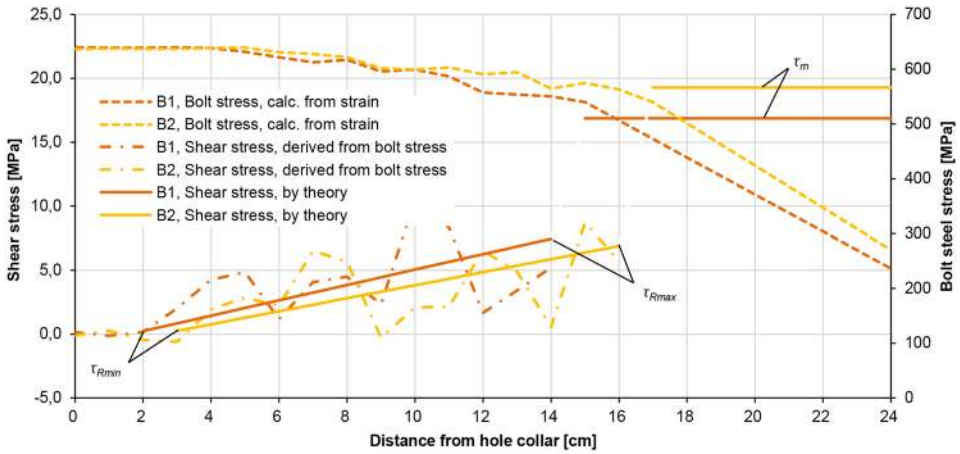

Fig. 25 Axial bolt stress and bond shear stress for Type 3 pull-out tests; these were calculated using measured plastic strain values and the equations presented in Sect. 3.3

sliding calliper. Because small variations in strain have a large impact on the calculated stress (see the resulting shear stresses in Fig. 24 and Fig. 25), the calculated bolt stress fluctuated in a relatively large range. It is worth noting that measured strain is not necessarily strain at the time of pull-out, in the case of plastic deformation. Fluctuations in the measured strain may, for example, be caused by differences in the size and hardness of the mortar aggregate, which can lead to small local differences in bolt-grout bond strength or sliding gauge measurement errors. However, the measurement method used is believed to be suitable and adequate for proving the concept of pull-out mechanisms.

As shown in Fig. 23 through Fig. 25, residual bond shear strength is very low compared to peak shear strength. In its initial state, the grout has a firm mechanical grip on the ribs of the bolt, as well as creating a cohesive bond between the grout and the bolt. However, in its residual state, shear stress is associated with the degree to which the crushed grout fractures between the top of the ribs and the remaining grout around the bolt (see Fig. 4). Because of this, the resisting shear stress is believed to decrease as bolt movement increases. In addition, shear stress is sensitive to normal stress reduction on the bolt-grout interface. The large reduction in shear strength in the plastic embedment length is therefore believed to be due to a combination of the loss of normal stress due to the bolt bar's radial contraction and decreasing shear stress due to the crushing of the grout that results from movement of the bolt.

As seen in Eq. (11), critical embedment length is dependent upon steel strength parameters, bolt diameter and shear stress parameters. All shear strength parameters (i.e., τ_m, τ_{Rmax} and τ_{Rmin}) are influenced by grout properties and the surface profile of the bolt, and the latter two are also influenced by the deformation capability of the bolt, that is, its A_{gt}. Following the arguments above, a bolt with a higher A_{gt}, that is, one that elongates more per load increment during the hardening stage, also sees a larger reduction in residual shear strength due to the larger relative movement of the bolt bar in the grout and greater radial contraction. We can therefore infer that stiffer steel has a shorter plastic deformation length than softer steel. It is likely that the A_{gt} has a quite large impact on critical embedment length, but it is difficult to tell how significant this impact is, since these tests only investigated one type of steel.

Unsurprisingly, in the case of bolts with a 30 cm embedment length (i.e., B1, B2, B3, B4, S3 and S5), the force needed to pull the bolts out of the hole decreased as the w/c ratio decreased. This demonstrates that four main factors influence critical embedment length: the shape/size of the surface profile of the bolt, the grout w/c ratio, steel strength properties (i.e., F_y and F_u) and steel deformation capacity. However, other factors also play a role, such as bolt corrosion protection layers and grout aggregate sizes.

The tests conducted in this study showed that the bond is not damaged when subject to pull loads below the F_y of the steel, as long as the embedment length of the bolt is longer than the elastic critical embedment length. Bearing this in mind, neither the bolt steel nor the bolt-grout bond would be damaged when undergoing quality control pull tests on site, as long as the pull load used does not exceed the F_y of the bolt steel.

7 Conclusions

When a bolt is loaded above the yield strength of the bolt steel, a portion of the grouted bolt shank located inward from the borehole collar is subjected to plastic deformation, and the bolt becomes partially debonded from the grout on the plastically deformed segment. The residual shear strength on the yielded bolt segment is considerably lower than the original bond strength of the bolt. From this, we can infer that the critical embedment length of a bolt in situ, if it is loaded above the steel's yield strength, must be longer than that which is calculated using data from short bolt segment tests in a laboratory, since the latter bolts are not normally yielded under the applied pull load. The grout in the borehole collar fractures and a failure cone is formed in the grout under the pull load on the bolt, which also results in a shorter effective embedment length.

It is proposed that the critical embedment length of a grouted rebar bolt is the sum of three components: the length of the cone of broken grout at the borehole collar; the plastic deformation length (i.e., the yielded bolt segment) that bears the load increment from the yield strength to the ultimate strength; and the elastic deformation length that bears the yield load. This theory is useful for determining the necessary length of a bolt segment anchored in competent strata behind a widening joint and can help avoid rock blocks falling.

Acknowledgements The authors would like to thank Gunnar Vistnes and Torkjell Breivik for their assistance with the laboratory work.

Compliance with Ethical Standards

Conflicts of Interest The authors have no conflicts of interest.

References

Benmokrane B, Chennouf A, Mitri HS (1995) Laboratory evaluation of cement-based grouts and grouted rock anchors. Int J Rock Mech Min 32(7):633–642. https://doi.org/10.1016/0148-9062(95)00021-8

Bigaj-van Vliet AJ (1999) Structural dependence of rotation capacity of plastic hinges in RC beams and slabs. Delft University Press, Delft

Blanco Martín L, Tijani M, Hadj-Hassen F, Noiret A (2013) Assessment of the bolt-grout interface behaviour of fully grouted rockbolts from laboratory experiments under axial loads. Int J Rock Mech Min Sci 63:50–61. https://doi.org/10.1016/j.ijrmms.2013.06.007

Bulck S (2015) Numerical analysis of rebar pull-out behaviour in concrete using cohesive zone modelling. Eindhoven University of Technology, Eindhoven

Federation Internationale du Beton (2000) Bond of reinforcement in concrete, vol 10. FIB bulletins. Federation Internationale du Beton, Lausanne

Forbes B, Vlachopoulos N, Diederichs MS, Aubertin J (2020) Augmenting the in-situ rock bolt pull test with distributed optical fiber strain sensing. Int J Rock Mech Min Sci 126:104202. https://doi.org/10.1016/j.ijrmms.2019.104202

Gaztelumendi DE (2012) Bond behaviour and tension stiffening of flat stainless steel rebars with continuous or alternate rib pattern embedded in concrete. Ghent University, Ghent, Belgium

Corporation IBM (2016) IBM SPSS statistics, 24th edn. IBM Corp, Armonk, NY

Kılıc A, Yasar E, Celik AG (2002) Effect of grout properties on the pull-out load capacity of fully grouted rock bolt. Tunn Undergr Sp Tech 17(4):355–362. https://doi.org/10.1016/S0886-7798(02)00038-X

Li CC, Høien AH, Kristjansson G (2016a) Critical embedment length of fully grouted rebar bolts. In: Paper presented at the Eighth International Symposium on Ground Support in Mining and Underground Construction, Luleå, Sweden

Li CC, Kristjansson G, Høien AH (2016) Critical embedment length and bond strength of fully encapsulated rebar rockbolts. Tunn Undergr Sp Tech 59:16–23. https://doi.org/10.1016/j.tust.2016.06.007

Li C, Stillborg B (1999) Analytical models for rock bolts. Int J Rock Mech Min Sci 36(8):1013–1029. https://doi.org/10.1016/S1365-1609(99)00064-7

Standard Norge (2012) Steel for reinforcement of concrete—Dimensions and properties—Part 3: Ribbed steel B500NC, vol. NS 3576–3. Standard Norge, Lysaker

Ren FF, Yang ZJ, Chen JF, Chen WW (2010) An analytical analysis of the full-range behaviour of grouted rockbolts based on a tri-linear bond-slip model. Constr Build Mater 24(3):361–370. https://doi.org/10.1016/j.conbuildmat.2009.08.021

Vlachopoulos N, Cruz D, Forbes B (2018) Utilizing a novel fiber optic technology to capture the axial responses of fully grouted rock bolts. JRMGE 10(2):222–235. https://doi.org/10.1016/j.jrmge.2017.11.007

Yeih W, Huang R, Chang JJ, Yang CC (1997) A pullout test for determining interface properties between rebar and concrete. Adv Cement Base Mater 5(2):57–65. https://doi.org/10.1016/S1065-7355(96)00004-1